Lithographic Regulation of Cellular Mechanical Properties

By

Tsu-Te Judith Su

B.S., Mechanical Engineering (2002)

Massachusetts Institute of Technology

Submitted to the Department of Mechanical Engineering
in Partial Fulfillment of the Requirements for the Degree of
Master of Science in Mechanical Engineering

at the

Massachusetts Institute of Technology

June 2004





Signature of Author.....
Department of Mechanical Engineering
May 7, 2004

Certified by.....
Peter T.C. So
Associate Professor of Mechanical and Biological Engineering
Thesis Supervisor

Accepted by.....
Ain A. Sonin
Chairman, Department Committee on Graduate Students

# Lithographic Regulation of Cellular Mechanical Properties

by

Tsu-Te Judith Su

Submitted to the Department of Mechanical Engineering
on May 7, 2004 in Partial Fulfillment of the
Requirements for the Degree of Master of Science in
Mechanical Engineering

## ABSTRACT

A magnetic trap in combination with two-photon fluorescence microscopy was used to determine the cytoskeletal stiffness and three-dimensional (3D) cytoskeletal structure of NIH 3T3 fibroblast cells plated on micropatterned substrates. Microcontact printing of self-assembled monolayers (SAMs) of alkanethiolates on gold was used to create a planar substrate of islands surrounded by non-adhesive regions. The cells were physically constrained within nanometer high adhesive cylindrical posts of defined size on the surface of a titanium and gold coated coverslip. The islands were coated with the extracellular matrix protein fibronectin (FN) and a protein inhibiter was used to restrict cellular extension. After plating, the cells were fixed and stained with phalloidin. A high-speed, two-photon scanning microscope was used to resolve actin architecture in three dimensions and a fractal dimension measurement was performed to quantify the distribution of actin within the cell as a function of adhesion area. The experiments intend to test the hypothesis that cytoskeletal mechanical properties are a function of cellular adhesion area. We further try to understand these mechanical changes by seeking a correlation between these mechanical parameters and actin stress fiber distribution. It was discovered that the fractal dimension is a weak inverse function of cell adhesion area but that there is a significant change in fractal dimension between patterned and control cells which can freely spread to their natural dimensions. Microrheological experiments using the magnetic trap show that the mechanical properties of patterned cells are similar within statistical error while significantly softer than the control cells.

Thesis Supervisor: Peter T.C. So
Title: Associate Professor of Mechanical and Biological Engineering

# Contents

# Acknowledgements

I would like to first thank my thesis advisor, Prof. Peter So for his guidance, support, and encouragement. In addition I would like to thank the members of the Bioinstrumentation Engineering and Microanalysis (BEAM) lab who have all answered my questions from time to time, but in particular Michael Previte for all his help which is too numerous to list, and Hyuk-Sang Kwon for helping with the magnetic trap holder and the machining, heat treatment, and wrapping of the magnetic trap. I would also like to thank Prof. George Whitesides for kindly inviting me to his lab to learn microcontact printing and Justin Jiang for demonstrating for me soft lithographic techniques and answering my questions. Finally, I would like to thank Jan Lammerding for the particle tracking program and other Matlab assistance and Kurt Broderick of the Microsystems Technology Laboratory (MTL) for training and assisting me on the e-beam, spin-coater, and mask-aligner.

This work is funded in part by a National Science Foundation (NSF) graduate research fellowship and NIH PO1HL64858.

# Chapter 1

# Introduction

## 1.1 Background and motivation

### 1.1.1 Overview

Cellular migration of adherent cells over surfaces is important for a wide variety of processes such as wound healing, tissue repair, vertebrate embryonic development, tumor angiogenesis and metastasis [1, 2]. The outline of how cellular processes are involved to create whole cell movement has been developed; however, the underlying mechanism of how individual molecular components temporally and spatially combine to orchestrate large scale movement remains unsettled. Cellular movement of adherent cells across a surface is chiefly guided by the attachment of the cell to the substrate. During wound repair, for example, initially stationary fibroblasts mobilize and crawl in a network of macromolecules known as the extracellular matrix (ECM) in order to migrate into the wound [3]. It has been demonstrated that the degree of adhesion of a cell to the extracellular matrix through transmembrane proteins known as integrins governs the speed and direction of cellular locomotion [4]. Controlling the cell-surface interaction and quantifying the resulting effect on cellular mechanical properties, which in turn regulate migration, provides one way to better understand how molecular components integrate to effect and regulate whole cell movement [5]. Soft lithographic techniques such as microcontact printing provide a molecular means of controlling the cell-surface interaction by creating a tissue culture substrate of nanometer high islands coated with extracellular matrix proteins to which a single cell may adhere with focal contacts [6]. Due to non-adhesive regions around the islands, the cell may only extend to take on the shape of the underlying island and as a result, the controlling role of cell size and shape and their relation to cellular function may be quantified, separate from other aspects of cell adhesion. This technique also provides insight into the first stage of cell migration, the mechanical state of a stationary cell. Quantification of a resting cell's mechanical properties, using substrate geometry to define the supporting boundary conditions, in addition to serving as the first step in studying cell migration, has potential implications in the development of cellular biosensors, tissue engineering principles, and understanding the basic biology as well as designing therapeutics for a number of cardiovascular diseases such as atherosclerosis and hypertensive vasculopathy. We hypothesize that because adhesion area dictates the placement of focal adhesion complexes and therefore the actin structural network, that we can regulate the mechanical properties of a cell by controlling its adhesion area. Through the use of microcontact printing, we seek to (1) use a single-pole magnetic trap to establish a relationship between the mechanical properties of stationary fibroblast cells and adhesion area and (2) use two-photon fluorescence microscopy to visualize in three dimensions and quantify the stress fiber distribution of fixed cells on artificial, micropatterned substrates.

### 1.1.2 The form of fibroblast motility

Fibroblast cells crawl by repetitively extending, attaching, contracting, and detaching from a surface. The leading portion of the cell membrane spreads and extends, forming a thin flattened structure known as a lamellipodium which adheres to the substrate and forms focal adhesion points. Contractile stress fibers within the cell link to the focal adhesion points in order to generate traction that pulls the bulk of the cell forward. Simultaneously the rear portion of the cell detaches and retracts. The leading edge of the cell, in order to move the cell forward, must be capable of sustaining a greater force than the tailing edge. This occurs either due to an increase in the number of focal adhesion points or an increase in the bond strength of each individual contact point [7].

Fibroblast cells typically migrate in the shape of an elongated triangle with the leading edge as the base. This breaking of symmetry due to the extension of lamellipodia causes differences in cellular function between the leading and trailing edge and gives cell movement a directional persistence and bias. Cellular movement which follows the routine of polarization, attachment, and detachment is known as fibroblast locomotion [8].

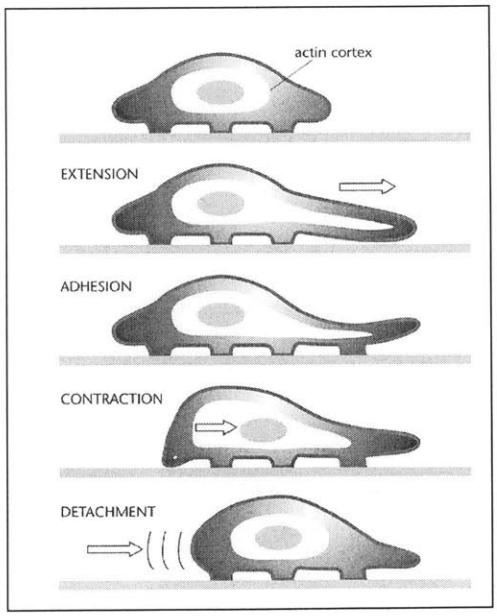


Figure 1-1: Schematic of cell migration over a surface [8].

A typical fibroblast cell is on the order of 20 $\mu$m and moves at rates of up to 40 $\mu$m /hr. The lamellipodia are wide but thin (0.1-0.4 $\mu$m tall) and rest on the focal adhesion complexes which hold the cell membrane 15 nm from the substrate [8]. Reflection interference microscopy has revealed that focal adhesions are 1-2 $\mu$m long. A detailed review of the molecular basis of cellular movement which includes active force generation on the molecular level may be found in [8].

### 1.1.3 The relation between cellular mechanical states and migration

Migration occurs in response to external cues which cause changes in cellular mechanical properties through cellular signaling pathways. Large scale cellular movements are generated by reorganization of the cytoskeleton. The cytoskeleton is a deformable intracellular filamentous protein structural network comprised of actin microfilaments, microtubules, and intermediate filaments. The mechanical properties of the cytoskeleton such as elasticity and bending modulus give the cell shape and stiffness and are also responsible for the traction force necessary to move the bulk of the cell during migration. Adherent cells in the first stage of migration mechanically sense their environment and transmit forces through focal adhesion points that are linked to the stress fibers of the cytoskeleton. Average contact stresses for migrating fibroblasts have been experimentally measured by measuring the displacement of small beads in an elastic substrate and have been found to range from 2,000-10,000 $N/m^2$ [9].

The extension and retraction of the cell membrane during migration is believed to be made by the polymerization and three-dimensional rearrangement of actin microfilaments [8]. Electron microscopy has revealed that the main cytoskeletal structural component in the lamellipodia is actin microfilaments which are approximately 7-9 nm in diameter [8]. In addition, because purified networks of actin polymers exhibit a higher shear modulus than networks containing microtubules or intermediate filaments, actin microfilaments are believed to be primarily responsible for the stiffness of the cell [2]. Actin may exist in filamentous (F-actin) or globular (G-actin) form [10]; however, only half of the actin filaments are present in the leading edge of the cell membrane. The remaining half form organized parallel bundles known as stress fibers. In fluorescence microscopy only the stress fibers and not the individual actin filaments are large enough to be visible [10]. Since the stress fibers adhere to the extracellular matrix through focal adhesion complexes, they may serve a mechanosensing function by transmitting and distributing forces from their environment. This mechanical interaction between the stress fibers and the extracellular matrix may determine cellular functions such as the direction and speed of which cells move.

We will use lithographic means to regulate the mechanical properties of a cell at zero velocity and see the end result by (1) visualizing and quantifying the distribution of stress fibers as a function of cellular adhesion area and (2) using a single-pole magnetic trap to apply a quantifiable force and measure the extent of the resulting time dependent deformation. The means by which the applied force is transduced into a chemical signal that ultimately changes and tunes the rigidity of the cytoskeleton is known as mechanotransduction and is the subject of future study. Experiments by Ingber have demonstrated that increasing the force applied to a cell using magnetic twisting increases the stiffness of the cytoskeleton [10]. A number of models which have been used to represent and understand cytoskeletal mechanics are described in section 1.1.5 and a detailed review of mechanotransduction may be found in [11, 12, 13]

### 1.1.4 The role of shape -- lithographic regulation of cellular mechanical properties

As described in sections 1.1.2 and 1.1.3, cell shape and adhesion play a crucial role in determining the mechanical properties of a cell and thus its ability to migrate.

Microcontact printing is a soft lithographic technique that can control the position, shape, size, and adhesion of a cell by manipulating the biochemistry and topology of the substrate [14]. This technique is based upon the patterning of self-assembled monolayers of alkanethiolates on gold and is described in greater detail in section 2.1.2.

Altering the morphology of a cell has been shown to control cell growth and function in culture; more specifically, cell size and shape has been shown to regulate proliferation, protein synthesis, differentiation, apoptosis, and cell phenotype [14, 15, 16]. Whitesides and coworkers demonstrated in 1997 that the cells could be switch from life to death by changing the adhesion area of cells [17]. In general, cells spatially constrained to a small area undergo apoptosis while cells on larger islands live. This switch from life to death as adhesion area decreased was also accompanied by a decrease in DNA synthesis and nuclear spreading. Further experiments by Ingber, Whitesides, and coworkers have demonstrated that controlling cell adhesion area dictates where cells form focal adhesion and exert the greatest tractional stress [18]. As cells exert the greatest stress just behind the main forward-extending lamellipodia, microcontact printing may also be applied to dictate where the leading edge of a cell forms. Recent work by these groups further shows that square cells extend lamellipodia preferentially from their corners [19] thus demonstrating that spatial cues guide the process of migration. In addition, fluorescence visualization has shown that in two dimensions stress fibers and focal adhesions redistribute and align preferentially along the edges of a particular patterned cell [20]. Adhesion area as regulated by microcontact printing is believed to alter the mechanical force balance of the cytoskeleton due to the forced distortion of the cell, but this hypothesis has yet to be proven directly [19].

### 1.1.5 Representing and modeling the mechanical properties of the cytoskeleton

The representation and modeling of the mechanical properties of the cytoskeleton has recently received a great deal of attention in the literature. The simplest representation of cytoskeletal mechanics approximates the cell as a continuum and uses spring and dashpots to represent the viscoelastic behavior of the cell [9]. The three main continuum cell models, each of which contains a different combination of springs and dashpots, are the Maxwell fluid, Voigt solid, and standard linear solid (Kelvin). The Maxwell fluid model contains a spring and dashpot in series, the Voigt solid contains a spring and dashpot in parallel and the Kelvin model consists of a spring and dashpot in parallel with another spring [9]. Each combination provides a different time-dependent viscoelastic response and additional responses may be modeled by adding more springs and dashpots.

There are micro-structural models which take into account how the actin microfilaments, intermediate filaments, and microtubules contribute to the elasticity of cytoskeleton. Because each model gives varying predictions for the mechanical behavior

of the cytoskeleton (Figure 1-2), no conclusions may be drawn about the validity of the models until more definitive experiments may be performed. We believe that performing experiments on patterned cells allow for the boundary conditions to be precisely defined and more definite experimental results to be obtained.

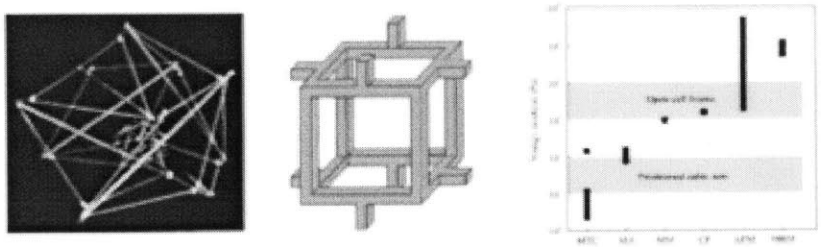


Figure 1-2: (a) Stick and strings model of a tensegrity structure [21] (b) A unit cell of the cellular solids model [22] (c) The wide range of elastic modulus as given by the tensegrity and cellular solids model for the structure of the cytoskeleton. The x-axis represents the different experimental methods used to measure the deformation of the cytoskeleton. From left to right: magnetic twisting cytometry, micropipette aspiration, microplate manipulation, cell poking, atomic force microscopy, and magnetic bead rheometry [23]

There are two commonly used micro-structural models for the cytoskeleton – the tensegrity model (Figure 1-2 (a)) proposed by Ingber and the cellular solids or open foam model (Figure 1-2 (b)) developed by Satcher and Dewey [9]. In the tensegrity model, the structural integrity of the cytoskeleton is maintained by the interaction of actin filaments in tension and microtubules in compression. The pre-stress in the cytoskeleton as a result of this interaction determines the deformability of the cytoskeleton. An in-depth review of the tensegrity model including mathematical formulations and how it predicts cell behavior and may be applied to understand mechanoregulation may be found in [21] and [22].

The cellular solids theory models low density cellular material by treating the cytoskeleton meshwork as a compilation of staggered unit cells connected at their midpoint by struts as shown in Figure 1-2 (b) [9]. When an external force is applied, the unit cell deforms and beam bending analysis may be used to extract values of the elastic modulus [23].

### 1.1.6 Quantifying the cytoskeletal distribution of a cell from fluorescent images

The cytoskeletal organization of a cell has been quantified by a variety of methods in order to objectively distinguish one cell from another and to determine the effect of various perturbations upon a cell. Visualization of the cytoskeleton by

fluorescence microscopy has become more common than high resolution electron microscopy in biological studies as fluorescence microscopy offers both the advantage of convenience and the ability to image live specimens. One common method of quantification of the digital images obtained from fluorescence microscopy has been to take the average fluorescence intensity in segments of the image and to normalize this number by the perimeter of the cell [23]. Intracellular shape recognition has been accomplished by calculating the distribution of the fluorescence intensity through moment invariant calculations. Other image processing and analysis techniques involve image interpretation algorithms which automatically characterize the orientation, size, spatial distribution [24], connectivity, and degree of complexity of the cytoskeleton [25] based on the pattern recognition of distinctive features such as the rod like or curved appearance of a particular fiber. The space filling property of the cytoskeleton may also be quantified by calculating the fractal dimensions of the image.

## 1.2 Objectives

In this work we use substrate geometry as a perturbative parameter to (1) measure the cellular mechanical properties (storage and loss moduli) under forcing using a magnetic trap and (2) quantify the three dimensional stress fiber distribution of patterned and control cells, which are unrestrained and are allowed spread under sub-confluent condition. Chapter 1 describes the background and motivation including a review of cell migration, how it links to cellular mechanical properties and the lithographic regulation of these properties. In chapter 2 we describe the materials and methods including soft lithography, magnetic trap, two-photon fluorescence microscopy, and sample preparation. Data, image analysis, and quantification and interpretation of results are discussed in chapter 3 and chapter 4 presents conclusions and suggestions for future work.

# Chapter 2

# Methods and Materials

## 2.1 Soft Lithography

### 2.1.1 Key features of soft lithography

Soft lithography is an inexpensive and rapid fabrication technique developed by George Whitesides and others to adapt existing photolithographic patterning techniques into biology. The three main techniques associated with soft lithography are microcontact printing, microfluidic patterning, and stencil patterning. Soft lithographic techniques eliminate the need for the expensive clean-room processing that conventional photolithographic patterning requires and does not require the use of chemicals which are toxic to cells [26]. A detailed review of soft lithography and its applications in biology is provided by Whitesides in [14]. Currently soft lithographic techniques can create features with a vertical height of 1 nm and a width as small as 30 nm [27, 28]. The two main features of soft lithography are (1) the development of methods for patterning chemicals on surfaces and (2) forming a soft polydimethylsiloxane (PDMS) stamp.

The first key feature of soft lithography is surface engineering. Soft lithographic techniques in combination with self-assembled monolayers of alkanethiolates on gold provide the ability to pattern organic molecules [14]. This allows a molecular level of control over surface properties. The tendency for organic thiol groups to form a dense array when reacted with gold has been well documented [28, 29, 30] and used extensively in biological studies. By chemically modifying the end group of the alkanethiol, it is possible to create surface monolayers whose properties can be mainly controlled by the end group. In this manner surfaces may be created with certain regions which selectively promote (addition of a methyl group) and certain regions which resist (addition of a polyethylene glycol group) the absorption of proteins. The creation of a protein adhesive monolayer island surface surrounded by a protein resistant monolayer surface may be used to control the size, shape, and location of anchorage dependent cells [14].

The second key component of soft lithography is the formation of a PDMS structure using replica molding. PDMS is an optically transparent, biologically compatible soft silicone elastomer whose surface properties may be easily modified [14]. The master mold is formed using conventional photolithographic techniques. To make the mask required, Whitesides and coworkers originated the concept of using a transparency or microfiche of a photographic negative as an inexpensive way to create a photomask [14]. Standard photolithographic techniques are then used to pattern a light sensitive polymer known as photoresist and create the master mold. The PDMS is then poured into the master mold and baked to create a soft biocompatible structure. In this manner, networks of microfluidic channels and stamps for microcontact printing (described in section 2.1.2) may be created. PDMS is also used in stencil patterning to

form a thin rubber sheet with holes in the shape of the desired pattern. Cells may be confined to grow within the holes and when the stencil is removed will retain the imposed shape for several hours.

### 2.1.2 Engineering Cellular Interactions by Microcontact Printing

Microcontact printing is a soft lithographic cellular patterning method based upon the printing of alkanethiolates on gold and has applications in the development of cellular biosensors as well as fundamental biological cell-substrate studies. There are two main steps in microcontact printing (1) the creation of a soft, biocompatible mold of the desired patterns and (2) the transferring of the patterns to a gold coverslip.

This entire process may be completed within 24 hrs and is outlined in Figure 2-1. First, a two-dimensional layout of the desired patterns is created using a commercial computer drawing package and a photomask was printed onto a laser transparency by a commercial printer operating at 5080 dpi. The patterns are colored opaque with the rest of the transparency left clear. Ultraviolet light is shone through the transparency onto a silicon wafer spin-coated with negative photoresist. The height of the photoresist is determined by the minimum horizontal feature size. Everywhere the light hits the photoresist polymerizes and hardens. Because the patterns are opaque and block light, only the regions around the patterns develop and solidify. The undeveloped photoresist is washed away using a photoresist developer leaving gaps in the photoresist of the patterns and creating what is known as the photoresist master (Figure 2-1).

**Step 1:** Creation of a photomask with desired patterns

**Step 2:** Preparation of titanium and gold coated substrates by electron beam vapor deposition

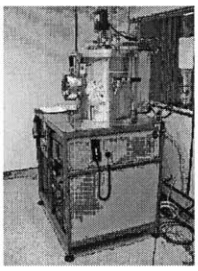

**Step 3:** A polydimethylsiloxane (PDMS) stamp is created using standard photolithography techniques. The stamp is inked with an alkanethiol and brought in contact with the gold substrate to form a self assembled monolayer (SAM) island in the shape of the patterns

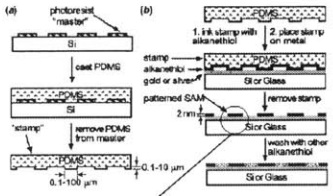


Whitesides, G.M., et. al (2001)

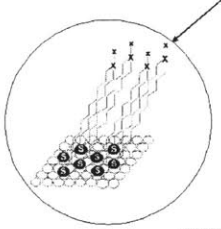

**Step 4:** The regions around the islands are coated with the same alkanethiol but with a polyethylene glycol (PEG) blocking group on the end. This prevents the adsorption of protein in the region around the islands.

**Step 5:** The islands are coated with fibronectin, an ECM protein, which promotes the adhesion of anchorage dependent cells. Therefore cells only stick to the islands.

**Step 6:** Cells are plated and are ready for visualization in three hours.

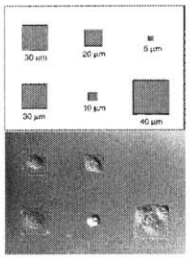


Chen, C.S., et. al (1997)

(a)

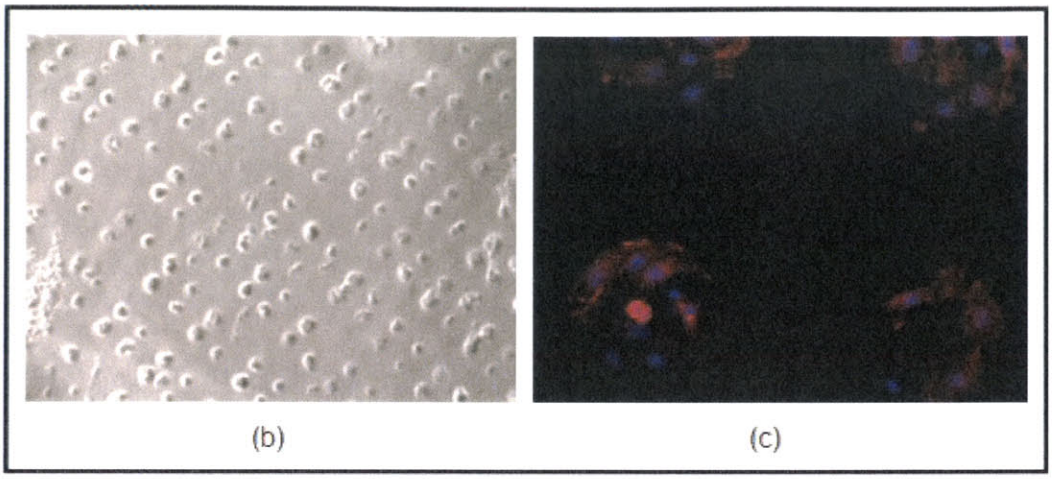


Figure 2-1: (a) Microcontact printing of alkanethiols on gold (b) an array of bovine endothelial cells on circular patterns (c) multiple fibroblast cells plated on circular patterns (nuclei stained with Hoechst and actin stained with rhodamine-phalloidin).

PDMS is then poured over the photoresist master to create a rubber stamp in the shape of the patterns. The stamp is then inked with an alkanethiol (in this case hexadecanethiol) and brought into conformal contact with a titanium and gold coated coverslip for 30 seconds and peeled off. The gold-thiol reaction causes the formation of 2-3 nm tall self-assembled monolayer (SAM) islands in the shape of the desired pattern. The patterns are transferred only where the stamp contacts the surface of the coverslip. These SAM islands are dense, crystalline structures which depending on the length of the chosen alkanethiol can be impermeable to water [14]. As a result, hydrophobic extracellular matrix proteins such as fibronectin preferentially adhere to the islands. To prevent cell extension beyond the islands the region around the islands is coated with a PEG-terminated alkanethiol for two hours creating another self-assembled monolayer which prevents the absorption of proteins. Anchorage dependent cells then selectively attach and are constrained to grow within the different sized planar adhesive islands (Figure 2-1 (b)-(c)). A more detailed description of this process may be found in section 2.2.1.

# 2.2 Visualizing the cell: two-photon fluorescence microscopy

## 2.2.1 Basic principle and advantages of two-photon microscopy

Two-photon excitation fluorescence microscopy (TPM) is a non-invasive three-dimensional visualization technique capable of imaging turbid biological specimens with submicron resolution [31]. A comprehensive review of two-photon excitation fluorescence microscopy which includes a detailed discussion of the physical principles of TPM and of the fluorescent probes used may be found in [31]. The principle of two-

photon excitation was first theoretically predicted in 1931 by Göppert-Mayer and was first used in combination with ultrafast pulsed lasers and a scanning microscope by Denk et al in 1990 to create two-photon excitation fluorescence microscopy. In TPM, a fluorophore is brought to an electronically excited state by the simultaneous absorption of two photons each with half the energy needed for the transition between the ground and excited state (Figure 2-2). Because molecules may be excited by TPM in the red to infrared, TPM can excite molecules which absorb in the ultraviolet (UV) and has the advantage of being less damaging to biological specimens than one photon fluorescence microscopy which typically excites fluorophores using only a single high energy UV photon (Figure 2-2). In addition because most tissues are transparent to the infrared, two-photon excitation has the added capability of deep tissue imaging [31]. The other advantages of two-photon microscopy over conventional one-photon microscopy are reduced photobleaching due to a reduction of the excitation region which is needed to increase the probability of the two photons spatially and temporally overlapping and the achievement of a higher signal to noise ratio due to the fact that the excitation and emission wavelengths are now further apart so that filters may separate them with minimal signal loss [31].

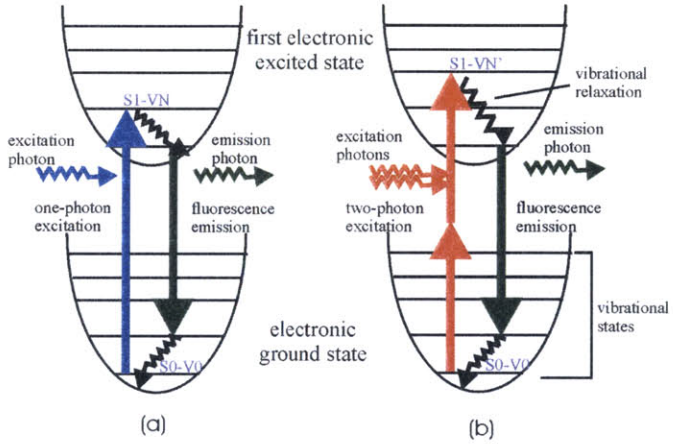


Figure 2-2: Jablonski (energy level) diagram comparing (a) one-photon excitation and (b) two- photon excitation. The horizontal lines represent vibrational levels within each electronic state. Due to vibrational relaxation after excitation, fluorescence emission occurs from the lowest vibrational energy level of the first electronic excited state and so is the same for both one-photon and two-photon excitation [31].

### 2.2.2 Two-photon fluorescence microscope design

A typical schematic of a two photon microscope is shown below in Figure 2-3.

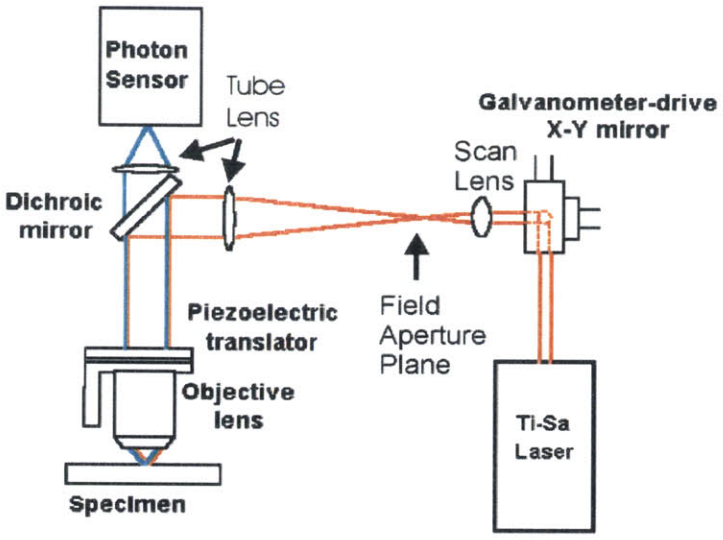


Figure 2-3: Schematic of a two-photon setup. The excitation light (red) may be filtered from the emission light (blue) by the use of efficient filters. [31]

The excitation light for two photon fluorescence is provided from a mode-locked Titanium-Sapphire laser (Mira 900, Coherent Inc., Palo Alto, CA) with a 150 fs pulse train and a 80Hz repetition rate. The laser beam power is controlled by a Glan Thompson polarizer and the attenuated beam is directed to the microscope (Zeiss Inc., Thornwood, NY) and focused through a scan lens by a galvanometer driven x-y scanner (Cambridge Technology, Watertown, MA). A dichroic mirror reflects the excitation light to the objective lens which focuses the light at a point on the sample. Images are generated by collecting the fluorescence emission generated by scanning the sample point by point. The fluorescence emission from the sample returns through the objective lens and is transmitted through the dichroic mirror to a tube lens that focuses the light on a photomultiplier tube (Hamamatsu, Bridgewater, NJ). A discriminator converts the optical pulse into electrical pulses which are counted and transferred to a computer which based on the number of pulses and their time of arrival can deduce the fluorescence intensity at each point and map them into an image.

# 2.3 Magnetic trap

## 2.3.1 General principles of a single-pole magnetic trap

The viscoelasticity of a cell has been measured by using a variety of different experimental techniques including deformation using optical tweezers [32], atomic force microscopy [33], magnetic bead rheometry [34, 38], and cell poking elastometer [35]. The application of a magnetic force to study the mechanical deformation of a cell was pioneered by Crick and Hughes in 1949 [36]. Magnetic twisting techniques which apply a torsional deformation to the cell have also been developed to study cytoskeletal stiffness [37].

A single pole magnetic trap was developed by Bausch, et al. in 1998 and has the advantage over other techniques of being able to exert comparatively large forces of up to 10nN on 4.5 $\mu$ m paramagnetic beads [38]. This allows the ability to deform the cytoskeleton of cells such as fibroblasts with elastic moduli calculated to be on the order of $10^3$-$10^4$ Pa [32]. The trap is an electromagnet that generates a magnetic field which exerts a quantifiable constant force $\vec{F}$ on a paramagnetic or ferromagnetic object,

$$\vec{F} = \frac{1}{2}\mu_0 \nabla\left(\vec{m} \cdot \vec{H}\right) \tag{1}$$

where $\mu_0$ is the permeability constant, $\vec{m}$ is the magnetization of the particle, and $\vec{H}$ is the external magnetic field strength. Generally paramagnetic as opposed to ferromagnetic beads are chosen as they only magnetize when the magnetic field is turned on and so are easier to control [38]. The beads are coated with fibronectin which allows them to indirectly attach to the actin cortex via integrin receptors on the cell membrane. By varying the current through the electromagnet, the amount of force applied to the bead may be controlled. Figure 2-4 shows the electronics schematic of the magnetic trap setup.

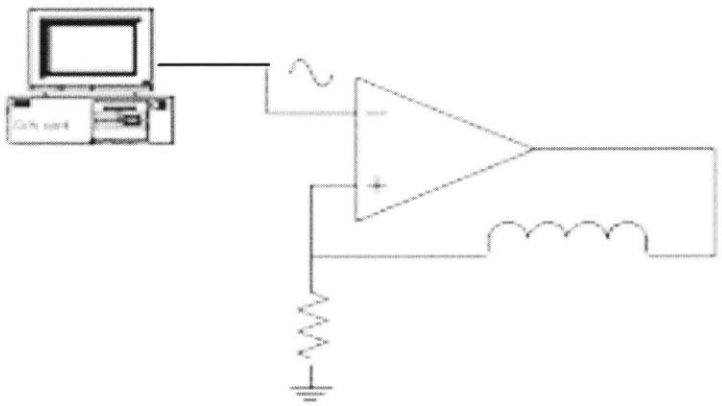

Figure 2-4: Schematic of electronics for magnetic trap setup. Waveform signal is amplified and sent through the inductor (magnetic trap) generating a magnetic field which exerts a force on the paramagnetic beads.

## 2.3.2 Experimental Setup

The single pole magnetic trap (Figure 2-4) was constructed following the design of [36] which used finite element simulations to maximize the force level. A paramagnetic CMI-C rod (Cold Metal Products Inc) was machined and heat treated to improve its magnetic properties. The trap was wrapped approximately 550 times with 21 gauge copper wire which was held in place by epoxy. The tip of the magnetic trap was

placed in the plane of the bead and cells were kept at 37°C through the use of a temperature controlled stage (Delta TC3, Bioptechs, Butler, PA).

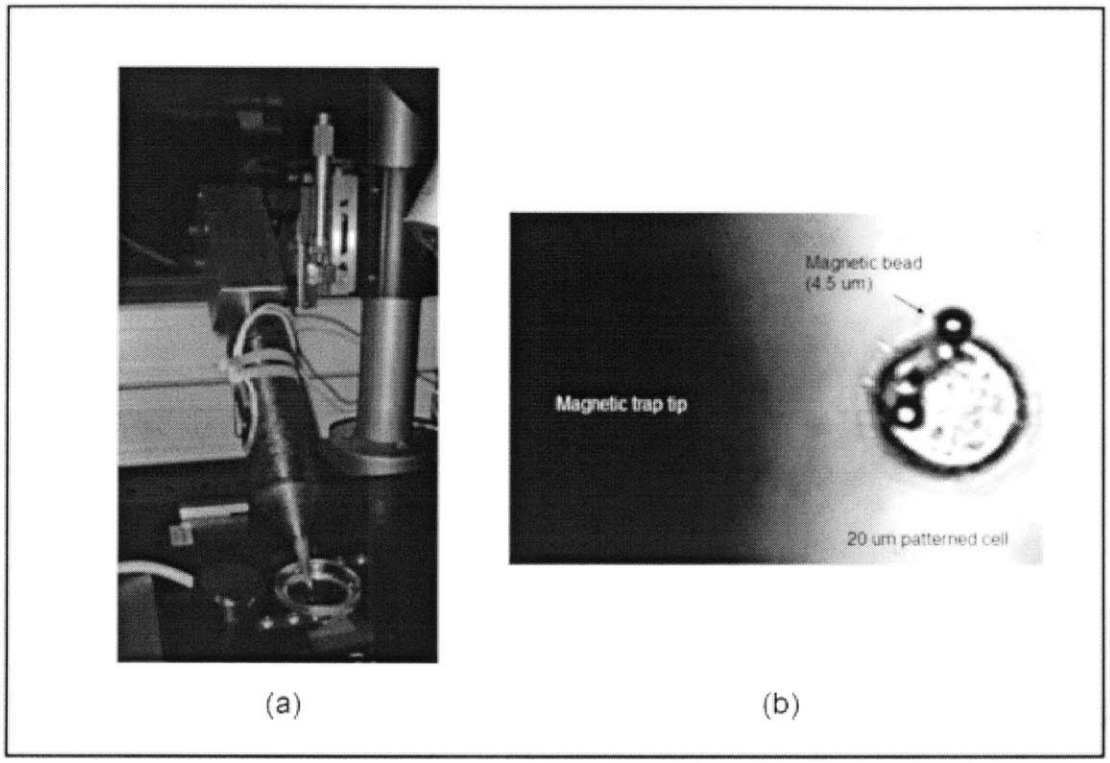


Figure 2-5: (a) Photograph of magnetic trap setup (b) Picture of 20 micron patterned cell with magnetic beads attached (63x magnification).

In each experiment a 5 second step forcing function of approximately 3nN of force was applied.

## 2.3.3 Calibration

The force on a bead associated with different current levels through the magnetic trap was determined by applying a force to a bead in a viscous solution and calculating the force using Stokes law. The solution used was dimethyl-polysiloxane which has a viscosity of 12,500 centistokes. The steady state velocity of the bead was found by measuring the displacement over time using a custom particle tracking program written in Matlab.

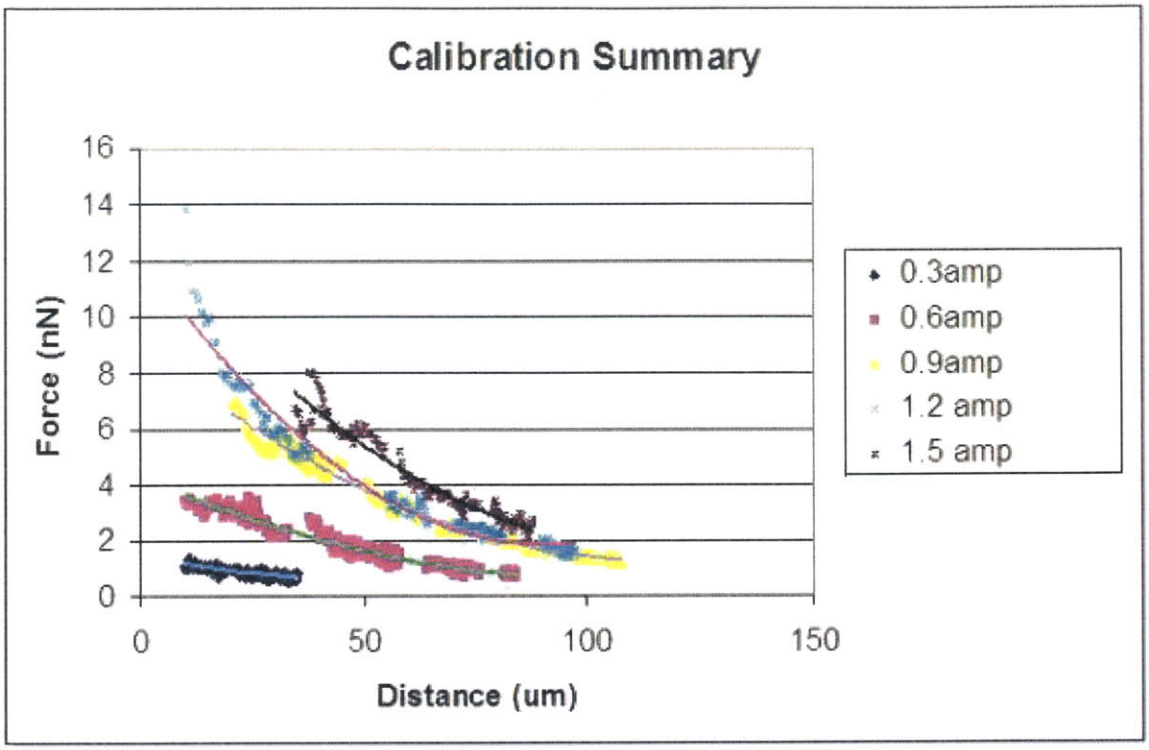


Figure 2-6: Force vs. distance calibration graph for different currents. Force was applied to 4.5 micron paramagnetic particles in polysiloxane. A general exponential function was used to determine the best fit to the data.

# 2.4 Sample preparation

## 2.4.1 Substrate preparation

115 angstroms of gold was deposited on sterile coverslips or bioptechs culture dishes (Bioptechs, Butler, PA) using electron beam vapor deposition. To promote the adhesion of the gold, 15 angstroms of titanium was first added. To create the PDMS (Sylgard 184, Dow Corning, Midland, Michigan) stamp using for microcontact printing, negative photoresist (SU8-2015, Microchem, Newton, MA) was spin-coated for 35 seconds at 1500 rpm onto a 4" silicon wafer. The photoresist was then baked on a hotplate at 65°C for 1 minute and 95°C for 2 minutes. UV light was shone on the photoresist for 12 seconds through a transparency photomask (Output City, Poway, CA) to create the photoresist master. Following the exposure the wafer was post-baked again at 65°C for 1 minute and 95°C. The unpolymerized photoresist was washed away with PGMA a photoresist developer and the wafers were silanized for 15 minutes to prevent the PDMS from sticking. PDMS was poured on top and baked in an oven for 2 hours at 65°C. The PDMS stamp (Figure 2-7) was then peeled off and coated with 2 mM hexadecanethiol (Sigma Aldrich, St. Louis, MO) in ethanol. The hexadecanethiol was evaporated off by blowing with nitrogen and the stamp with the evaporated vapors was pressed onto the gold coverslip for 30 seconds. The stamp was then gently peeled off and

the coverslip soaked in 2mM of a PEG-terminated alkanethiol (Prochimia, Poland) for no more than 2 hours.

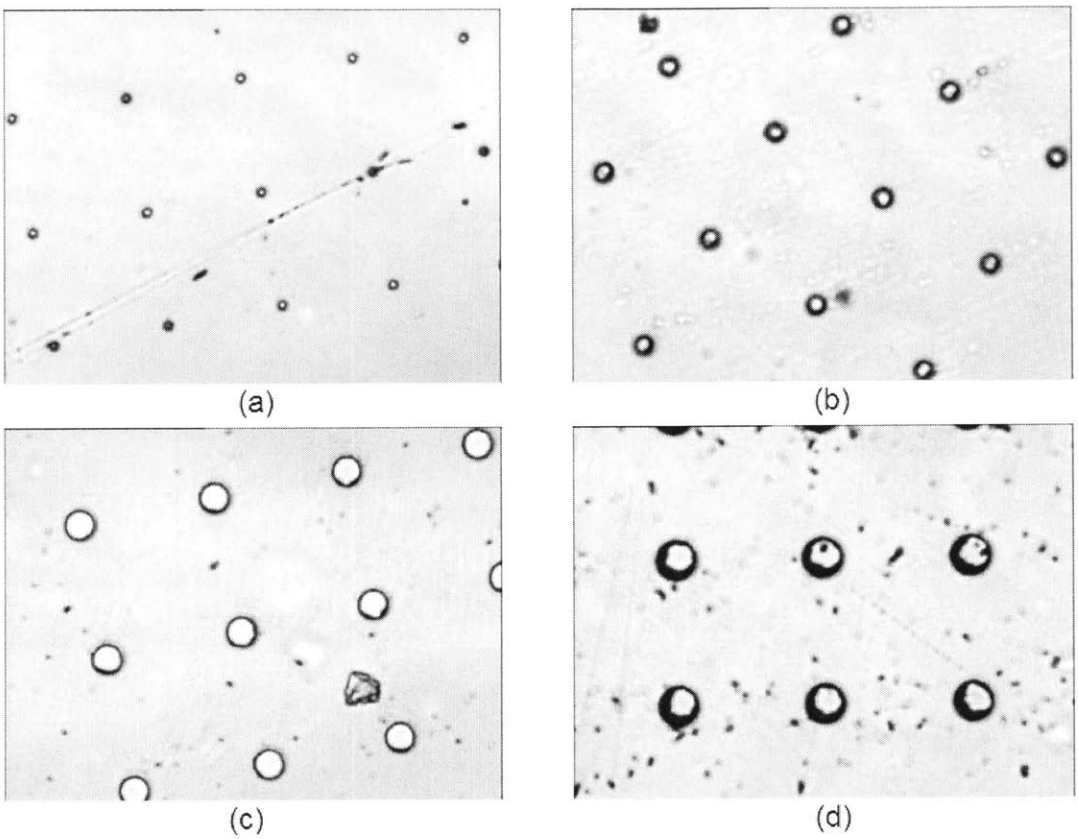


Figure 2-7: Photograph of PDMS stamp taken at 10x magnification (a) 10 micron circles (b) 20 micron circles (c) 30 micron circles (d) 40 micron circles. The posts are 10 microns tall and separated by 100 microns.

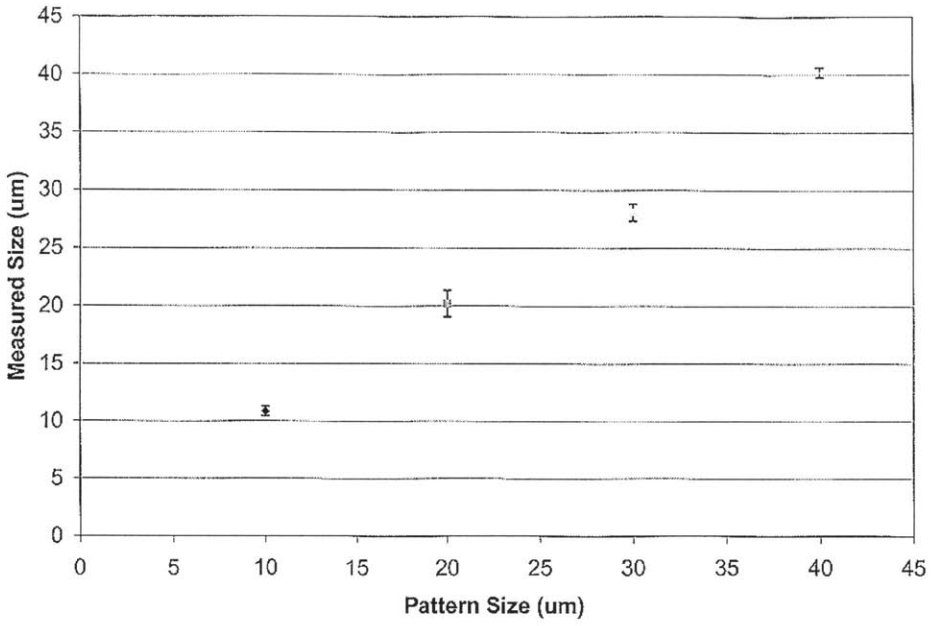


Figure 2-8: Desired pattern size versus actual pattern size of PDMS stamp. Each data point represents the average of five measurements. Error bars represent one standard deviation above and below the mean.

Because the islands are hydrophobic their presence may be visualized by breathing on them (Figure 2-9):

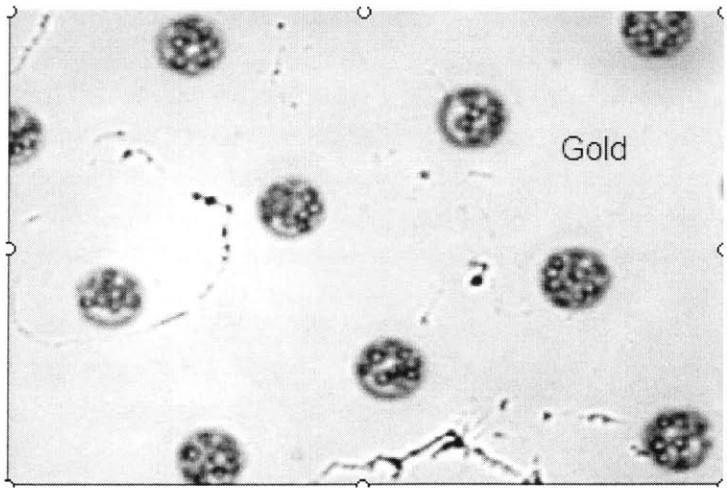


Figure 2-9: 40 micron circular patterns on a gold coverslip. The patterns are visualized by droplets of water vapor which attach to the hydrophilic surrounding area.

## 2.4.2 Cell culturing and plating

Cells were cultured according to instructions provided by the American Type Culture Collection (ATCC). NIH 3T3 fibroblasts (ATCC, Manassas, VA) were grown in $10cm^2$ tissue cultures plates in an incubator at 37°C until 70% confluent. The growth media used was high glucose Dubecco's Modified Eagle Medium (DMEM) supplemented with 10% v/v fetal calf serum (Invitrogen Life Technologies, Carlsbad, CA) and 1% penicillin/streptomycin. In a laminar flow hood, the media was vacuum aspirated off with a sterile pipette and 2.5 ml of trypsin-EDTA was added. The cells were placed back into the incubator for 5-7 minutes until the cells disassociated from the bottom of the plate. An equivalent amount of serum containing media was then added to inactivate the trypsin. The solution of media and cells was then gently mixed using a 5 ml pipette for several minutes until a homogeneous cell suspension was obtained. The desired amount of cells was then added to a new tissue culture plate for continued propagation and placed back into the incubator.

To plate the cells, the patterned gold coverslips were washed in ethanol, dried with a stream of nitrogen and placed in the bottom of a six well plate. Each coverslip was then soaked in 2 ml of 0.25 $\mu$g/ml of human plasma fibronectin in phosphate buffered saline (PBS) solution (Invitrogen Life Technologies, Carlsbad, CA) for a minimum of 30 minutes. The fibronectin was then aspirated out while the desired amount of cells was simultaneously pipetted in taking care not to expose any portion of the coverslip to air. For a 22 mm square coverslip approximately 30,000 cells were added per well. The cells are ready for visualization in approximately 3 hours.

## 2.4.3 Staining the actin

Cells were fixed with 3.7% formaldehyde (Z-fix, Anatech LTD, Battlecreek, MI) and their F-actin stained with Alexa Fluor 488 conjugated phalloidin (Molecular Probes, Eugene, Oregon) according to directions provided by Molecular Probes. The media was first aspirated and the cells were washed twice with PBS. Z-fix was added for 10 minutes and then aspirated off. The coverslips were washed again twice with PBS and a solution of 0.1% Triton X-100 was added for a total of 3-5 minutes to wash away the cell membrane and allow for the dye to enter. The Triton X-100 was removed, the coverslips washed twice with PBS, and the coverslips were soaked in a 1% bovine serum albumin (BSA) solution for 20-30 minutes to reduce non-specific binding. The staining solution consisting of 200 $\mu$l of PBS and 10 $\mu$l of methanolic dye solution was then added to each coverslip for 20 minutes after which the coverslips were washed again twice with PBS.

## 2.4.4 Magnetic bead preparation

4.5 $\mu$m paramagnetic polystyrene beads (Dynal, Oslo, Norway) with a tosyl-activated coating were covalently conjugated to fibronectin according to instructions provided by the manufacturer. The solution containing the magnetic beads was placed on top of a magnet to draw the beads to the bottom. The storage solution was then aspirated off and the beads washed once in a borate buffer solution with a pH of 9.4. 5 $\mu$g of

fibronectin were added for every $10^7$ beads and the solution was gently agitated for 15 minutes at 37°C. BSA was added until the solution was 0.1% BSA and the entire mixture was agitated overnight at 37°C. Afterwards, the beads were washed three times with 0.1% BSA in PBS and once with Tris buffer with 0.1% BSA (pH 8.5). Prior to use the beads were mixed in 1% BSA in PBS for 5 minutes and then resuspended in media. This mixture was added to the cells for at least two hours before experiments were performed.

# Chapter 3

# Results and Discussion

## 3.1 Two-photon images of patterned cells

Images of 10, 20, 30, and 40 micron cells were taken using two-photon fluorescence excitation microscopy at an excitation wavelength of 780 nm and 20 mw of power. The size range was chosen to be as wide as possible with the upper and lower limits being that if the islands were too small (~ 5 microns) the cells would undergo apoptosis and if the islands were too large then more than one cell would land on it. A 40x Fluar Zeiss objective was used for imaging. Two-dimensional slices were taken every 250nm for a total of 40-75 slices. Three-dimensional images (Figure 3-1) were reconstructed using Imaris.

For actin visualization, NIH 3T3 fibroblast cells were patterned on 10, 20, 30, and 40 micron circles. The cells were then fixed with formalin and stained with Alexa Fluor 488. Images were taken with two photon fluorescence microscopy at 40x magnification. Slices were taken every 250 nm for a total of 80 slices. 2D slices at the widest cross-section of the cell are presented: (a) 10 μm (b) 20 μm (c) 30 μm (d) 40 μm (e) control. Axes on picture represent number of pixels.

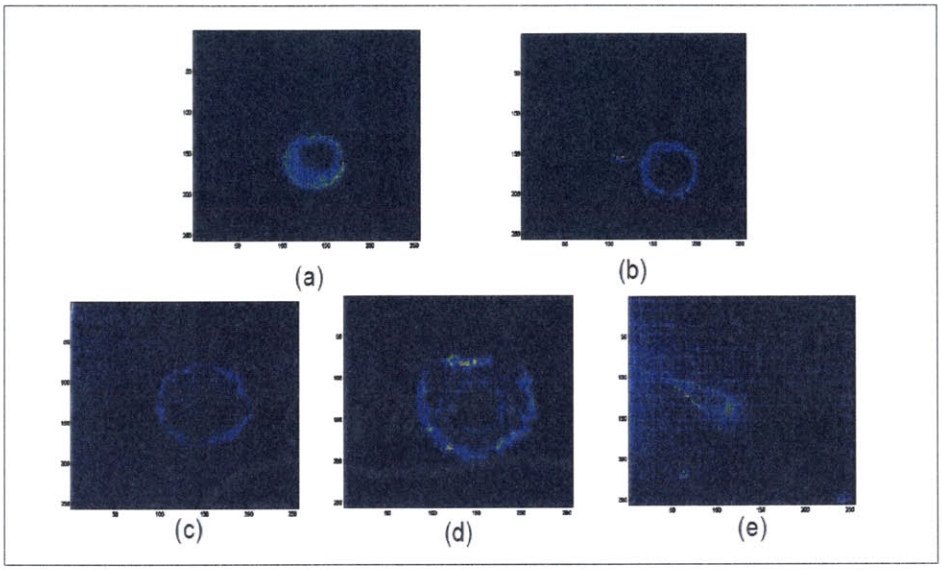


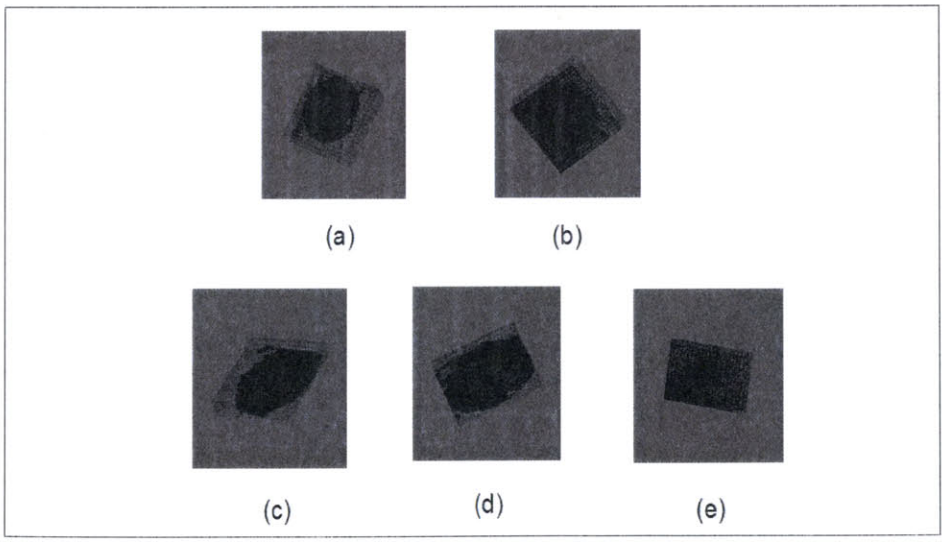


3D images were reconstructed using Imaris. Scale is not the same for each picture. (a) 10 μm circle (b) 20 μm circle (c) 30 μm circle (d) 40 μm circle (e) unpatterned cell

Figure 3-1: Two-photon fluorescent images of patterned cells.

## 3.2 Cytoskeletal architecture of patterned cells

### 3.2.1 Quantification of stress-fiber distribution

Images obtained by TPM were first thresholded to minimize the effect of background noise. One limitation of using two-photon imaging is that the gold substrate absorbs in the infrared thus creating a high intensity background luminescence which makes getting a clear picture of the cell at the attachment plane difficult. The effect of dark noise was calculated by taking the mean and standard deviation of intensity values for a background region clearly outside the cell. Values equal to and below 30 standard deviations above the mean of these background intensity values were set to zero. The three-dimensional stress fiber distribution of the patterned cells was then quantified by calculating the fractal dimension of each image by method of box counting.

### 3.2.2 Fractal dimension

The concept of fractal geometry was developed in 1975 by Benoit Mandelbrot who coined the word fractal from the Latin adjective fractus meaning broken and the corresponding verb frangere meaning to break into irregular fragments. Fractals are geometric patterns that repeat independent of scale and so magnified fragments of the image appear similar or identical to the whole image [40]. This statistical self-similarity may be quantified by the fractional or fractal dimensions of the object. The dimensions of a fractal may be grouped into three main categories – the fractal dimension (D) describes the how an object fills up space, the topological dimension describes the connectivity of points within an object, and the embedding dimension describes the space around the object. Fractals allow for the characterization of irregular natural shapes which cannot be easily characterized by Euclidean geometry as most regular shapes posses only a few characteristic lengths. A detailed description of fractal geometry with formal mathematical detail is provided by Mandelbrot in [41].

We quantified stress fiber geometry by calculating the fractal dimension of each image by method of box counting using Fractal Analysis System for Windows v. 3.40 [42]. In this manner the spatial arrangement of the fluorescent points was determined. A three-dimensional rectangular grid was created over the image and the number of non-empty boxes was counted. This measurement was repeated for increasing resolution by using boxes with sides half the size of the previous boxes. D is the slope of the logarithmic plot of the number of boxes needed to cover the image vs. the size of the box [40]. The fractal dimension describes at increasing resolution how many new pieces of the object may be seen and in addition corresponds to the concept of mass dimension which describes the amount of material some distance from a point [41].

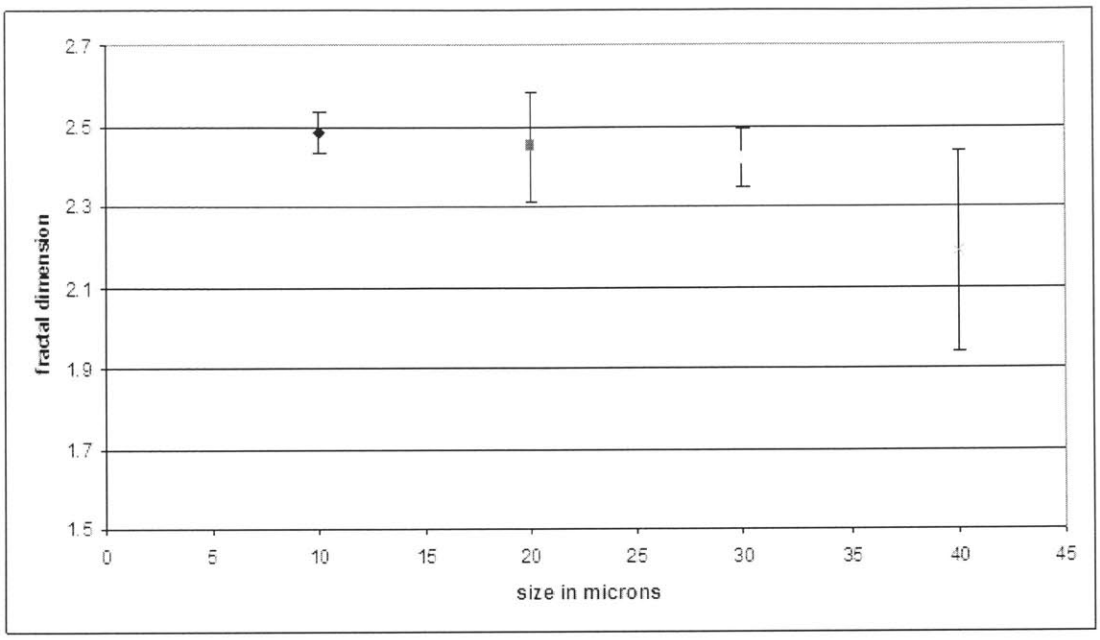


Figure 3-2: Fractal dimension (D) versus size of patterns in microns. Each data point represents the average of five repeated measurements. Error bars represent one standard deviation above and below the mean.

It was shown that smaller cells have a higher fractal dimension. A one-tailed unpaired t-test demonstrated a statistically significant ($p = 0.02$) difference in fractal dimension between the 10 micron patterned cell and the 40 micron patterned cell. Statistical significance was assumed for values $p < 0.05$. The fractal dimension was calculated for various threshold levels for background suppression demonstrating the trend to be threshold independent. As shown from the two-photon images and quantitatively from the fractal dimension, larger cells demonstrate a clustering of their stress fibers whereas the cortical actin distribution for the 10 micron cells appears to be continuous. Unlike the control cells which have stress fibers spreading throughout the length of the cell, the stress fiber distribution of the circular cells appear to be completely along the edges of the cell. The meaning of the fractal dimension may be seen in the fact that a fractal dimension of one corresponds to a line where a fractal dimension of two corresponds to a plane. Because the control cell contains long stress fibers which stretch throughout the cell, its fractal dimension is closer to one. The fact that the cell is three-dimensional gives the fractal dimension of the control cell a value slightly higher than one. Similarly in the case of the patterned cells, with a cortical actin distribution, the fractal dimension is slightly higher than two since the cell is 3D. Because the forty micron cell has a clustered appearance much like that of a broken plane, its fractal dimension is lower then that of the others. Magnetic trap experiments were conducted to test if these changes in fractal dimension corresponded with a change in cellular stiffness.

## 3.3 Quantification of patterned cell stiffness

To quantify the stiffness of the cells, magnetic beads were placed on a cell and pulled upon with approximately 3 nN of force for 5 seconds. A typical bead displacement response of a cell is shown below in Figure 3-3.

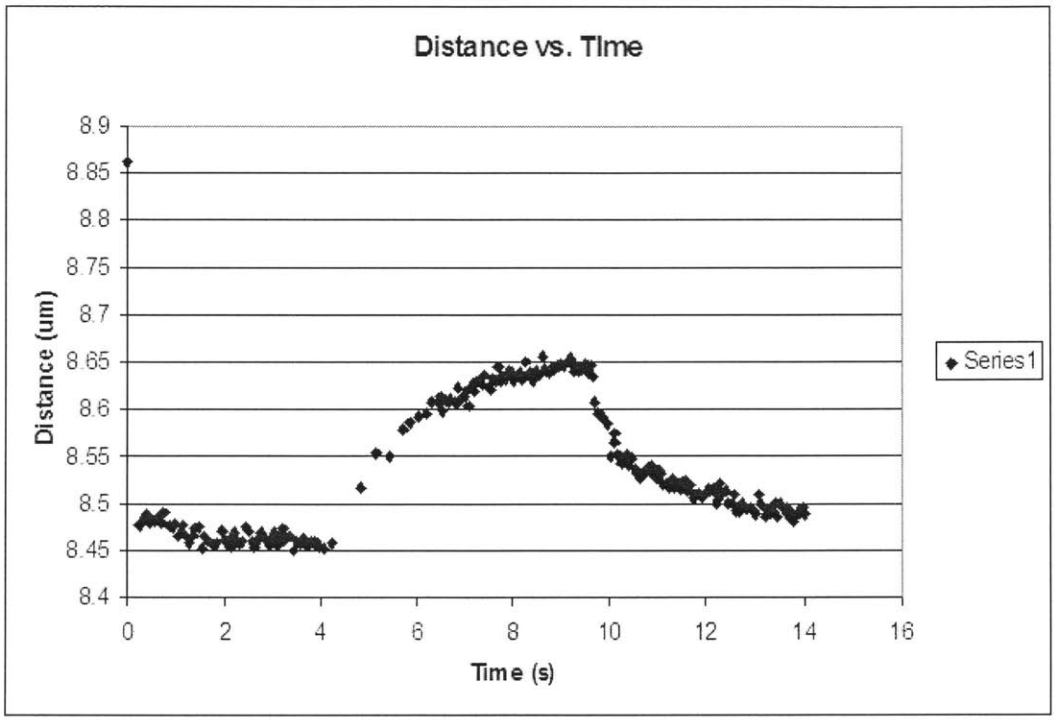


Figure 3-3: A representative creep response of a control cell.

The viscoelastic response of the cell was modeled using a Voigt model in series with a dashpot (Figure 3-4).

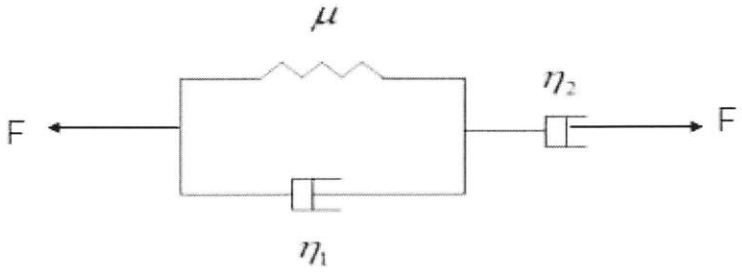


Figure 3-4: Voigt model in series with a dashpot.

Goodness of fit statistics shows the sum of squared errors to be typically around 0.002 and the $R^2$ value to be around 0.96 for this model. Figure 3-5 (a)-(c) plots as a

function of cell size the three parameters obtained from fitting the rising portion of the curve to the model.

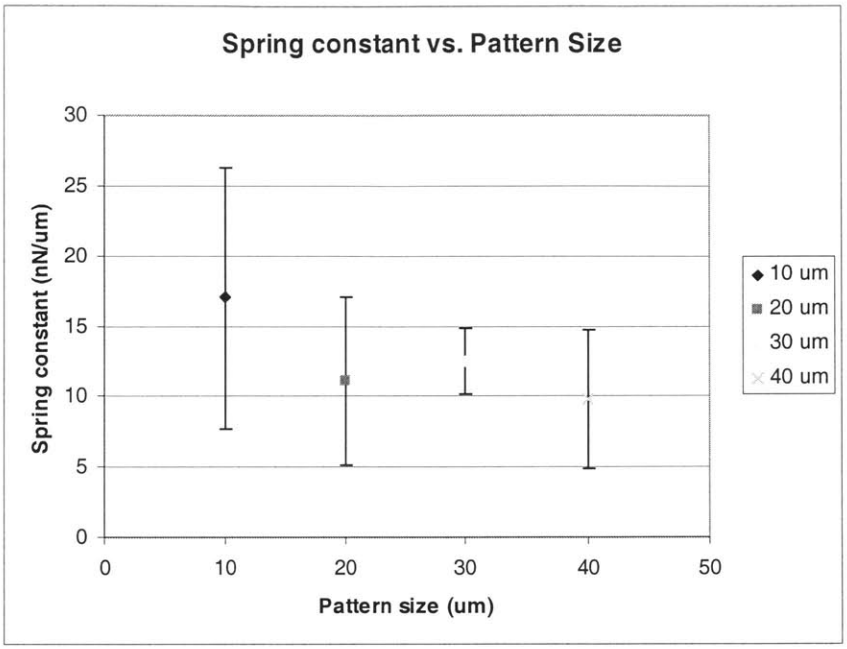


(a)

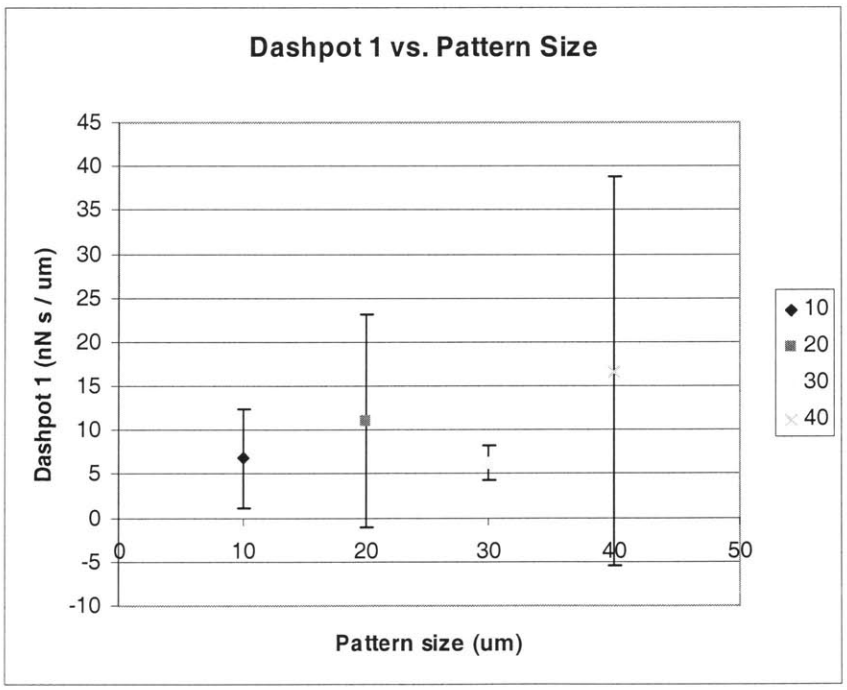


(b)

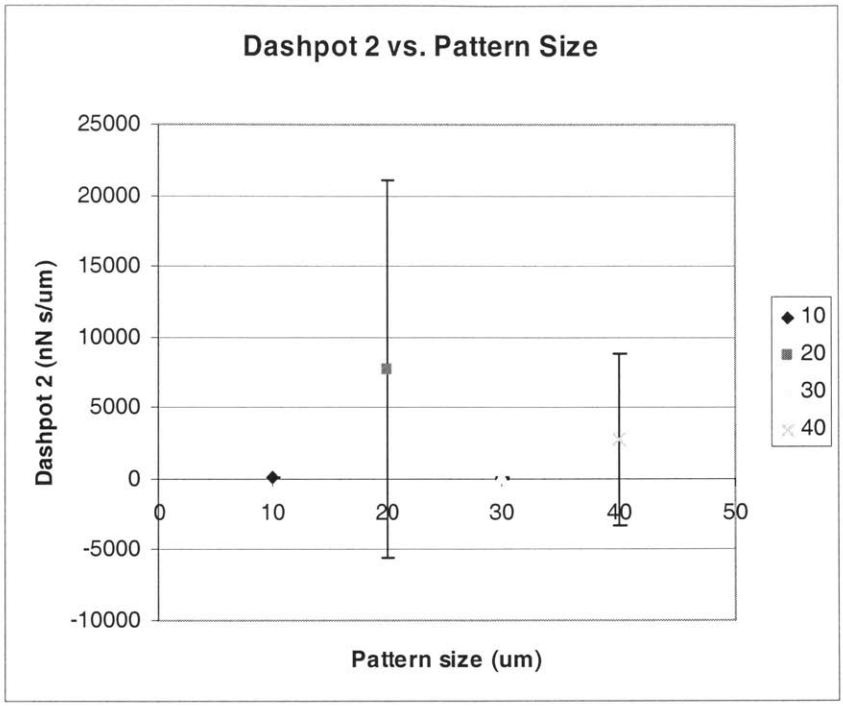


(c)

Figure 3-5: The viscoelastic response of the cell. The parameters were extracted from fitting the portion of the data during force application to a Voigt model in series with a dashpot (a) $\mu$ vs. pattern size (b) $\eta_1$ vs. pattern size (c) $\eta_2$ vs. pattern size. 7 data points were taken for the 40 micron circle, 5 data points were taken for the 30 micron circle, and 3 data points were taken for the 10 and 20 micron circle. Error bars represent one standard deviation above and below the mean.

As shown in the above figure, cell stiffness appears to be independent of adhesion area. Although the cell is an inhomogeneous dynamic system with functions such as life/death which can be regulated by the extent to which a cell can grow and spread, the fact that the stiffness remains unchanged as area increases is consistent with the notion of a homogeneous system whose properties scale with size. One possible reason could be that although there is a difference in fractal dimensions as pattern size increases, the actual difference in the value of the fractal dimension is small suggesting only a small change in the actin rearrangement and hence only a minor effect on the mechanical properties of the cell. In addition, since what we measure are the local viscoelastic properties of the surface of the cell these may or may not be affected by the bottom attachment plane. This is consistent with the notion that there exists a certain cutoff radius above which the mechanical properties of the cell are not significantly affected. Figure 3-6 plots the spring constant value obtained from the fit versus the fractal dimension (D) of the cells.

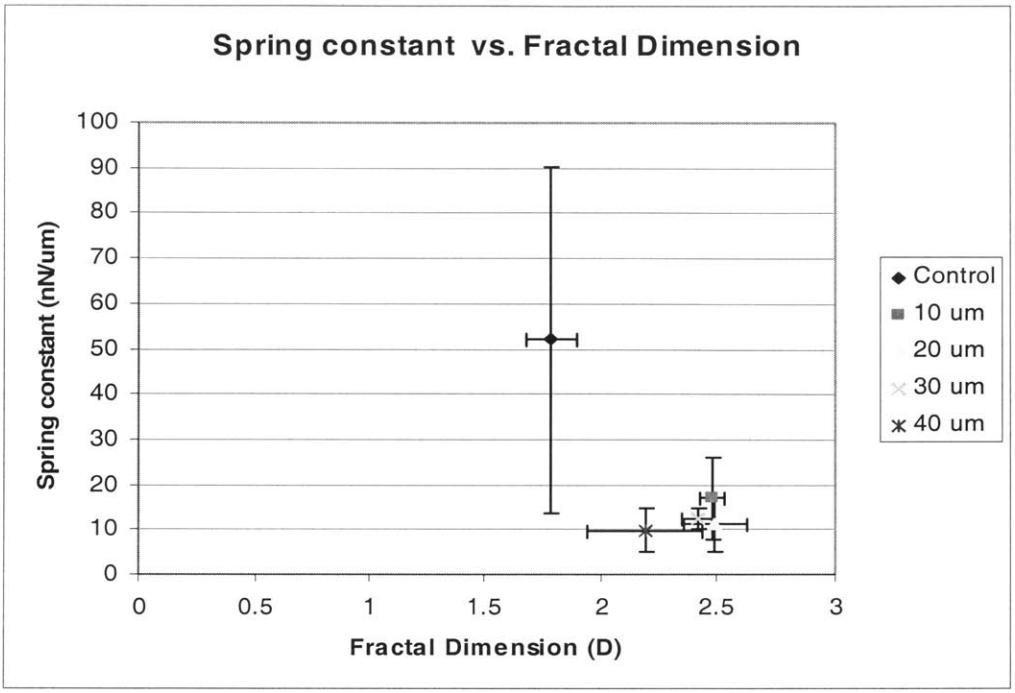


Figure 3-6: Spring constant (μ) vs. Fractal Dimension (D). Error bars correspond to one standard deviation above and below the mean.

From Figure 3-6, increasing fractal dimension correlates with a decrease in cell stiffness. There exists a statistically significant difference ($p = 0.17$) between the spring constants for the control cell and the spring constants for the patterned cells. In addition the patterned cells since they are more controlled display a much tighter distribution. One can explain why lower fractal dimensions may relate to higher cell stiffness if one accepts that the stress fiber network has a significant contribution in the mechanical stiffness of the cell. The better developed as well as parallel oriented stress fiber structure in the control cells results in their higher stiffness. Since there are almost no major stress fibers observed in the patterned cell and only a cortical distribution of actin is observed, one may expect a lower cellular stiffness. The limitations of this argument is that since only the stress fibers can be visualized by phalloidin staining, we cannot discuss what changes in other components of the cell such as the fine actin meshwork may or may not be responsible for triggering this response. Moreover we do not know whether the cortical actin distribution that we observe from fluorescent imaging is that of fiber bundles or a high density of the fine actin meshwork. To test whether or not stress fibers do play a significant role in determining the mechanical properties of a cell, we can repeat these experiment using square patterns instead and see if the spring constant and fractal dimension of these cells lies between that of the control cell and the circular cells. More pronounced stress fiber formation has been observed in square patterns where stress fibers mainly lie along the edges of the cell but also stretch across the diagonals of the square (Figure 3-7).

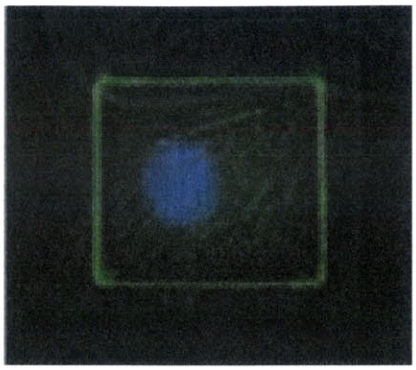

Figure 3-7: The stress fiber distribution of a square endothelial cell [19].

In addition, experiments may be conducted using cytochalasin D, a metabolite that blocks the formation of microfilament structures. Experiments by Ingber have demonstrated that the addition of cytochalasin D to cells results in a fivefold decrease in endothelial cell stiffness as measured by magnetic twisting. This change is comparable with our result that there is roughly a fivefold decrease in the spring constant that is shown in Figure 3-5 between the control cell and the patterned circular cells. This suggests but does not confirm that since the patterned cells with a circular actin distribution have a relatively low stiffness as compared to the parallel fibers of the control cells that it is the orientation of the stress fibers which may be significant in determining the mechanical properties of the cell.

# Chapter 4

# Conclusions and future directions

We examined the relationship between adhesion area and stress fiber distribution and whether those changes correlated with a change in cytoskeletal stiffness. As shown from the two-photon images, an increase in cellular adhesion area corresponds to a quantifiable rearrangement of the stress fiber distribution within fibroblast cells. Within the patterned cells this rearrangement is not enough to contribute to a change in the mechanical properties of the cell. There exists however a significant difference between the fractal dimension and spring constant of the control cells and the patterned cells. This difference may potentially be attributed to the absence of stress fibers across the cell in the circular patterned cells. One significant finding is that controlling the size and shape of the size greatly reduces the wide spread in the mechanical properties of the cell as is typically measured from unpatterned cells. This provides not only a means of engineering a cell in a specific mechanical state but a method of achieving better statistics in cell mechanics measurements. In addition, these experiments provide a means to clarify the controversial role of stress fibers in determining cytoskeletal stiffness. Immediate future work would include repeating the experiment for square patterns of the same area and seeing the effect of cytochalasin D on the stiffness on the symmetrical circular patterned cells. Because we hypothesize that it is the orientation of the fibers which are most important for the stiffness of the cell, adding cytochalasin D to circular patterned cells should result in a smaller decrease in stiffness then as found for similarly treated unconfined cells. Additional future work would involve SEM and transfecting cells such that the other structural components of the cytoskeleton such as the intermediate filaments and microtubules may be visualized and their distribution quantified as well. More information of the amount and distribution of these structures may be obtained by performing a three dimensional moment analysis in addition to a fractal dimension on each image. This would take into account the intensity of each point which is neglected in the fractal dimension measurement

# Chapter 5

# References


1. Eddy, R. et al., "Microtubule Asymmetry During Neutrophil Polarization and Migration," *Molecular Biology of the Cell*, Vol. 13, pp. 4470-4483, 2002.
2. Lauffenburger, D. and Horwitz, A. "Cell Migration: A Physically Integrated Molecular Process," *Cell*, Vol 84, pp. 359-369 (1996)
3. Lodish, H., et. al., *Molecular Cell Biology*, Freeman and Company., 2002
4. Palecek, S.P., et. al., "Integrin-Ligand Binding Properties Govern Cell Migration Speed Through Cell-Substratum Adhesiveness, " *Nature*, vol. 385, pp. 537-540, 1997.
5. Dalby, M.J., et. al., "Increasing Fibroblast Response to Materials Using Nanotopography: Morphological and Genetic Measurements of Cell Response to 13-nm-High Polymer Demixed Islands.", *Experimental Cell Research,* vol. 276, pp 1-9., 2002.
6. Park, T.H., et. al, "Integration of Cell Culture and Microfabrication Technology", *Biotechnol. Prog.,* vol 19, pp. 243-253, 2003.
7. Maheshwari, G., et. al. "Biophysical integration of effects of epidermal growth factor and fibronectin on fibroblast migration", *Biophys J.* vol 76, pp. 2814-2823, 1999.
8. Bray, D., *Cell Movements: From Molecules to Motility*, Garland Publishing, 2001.
9. Lo, C. M., et al. "Cell Movement is Guided by the Rigidity of the Substrate," *Biophys. J.* vol. 79, 144-152., 2000.
10. Alberts, B., et. al., *Molecular Biology of the Cell*, Garland Science, 2002.
11. Ingber, D.E., et al., "Mechanobiology and Diseases of Mechanotransduction", *Ann. Med.,* vol. 35., pp. 564-577., 2003.
12. Vogel, V. and Baneyx, G. "The Tissue Engineering Puzzle: A Molecular Perspective." *Ann Rev Biomed. Eng.* vol 5, pp. 441-463, 2003.
13. Davies, P.F., et. al., "Spatial Relationships in Early Signaling Events of Flow-Mediated Endothelial Mechanotransduction." *Ann. Rev. Physiol*, vol 59, pp 527-549, 1997.
14. Chen, C.S., et. al., "Micropatterned Surfaces for Control of Cell Shape, Position, and Function.," *Biotechnol Prog.* vol. 14, pp. 356-363. 1998.
15. Dalby, M.J., et. al., "Fibroblast Reaction to Island Topography: Changes in Cytoskeleton and Morphology with Time", *Biomaterials*, vol. 24, pp. 827-935, 2003.
16. Kane, R.S., et. al., "Patterning Proteins and Cells Using Soft Lithography", *Biomaterials,* vol. 20. pp. 2363-2376., 1999.
17. Chen., C.S., et. al., "Geometric Control of Life and Death", *Science.*, vol 276. pp. 1425-1428., 1997
18. Wang, N., et. al, "Micropatterning Tractional Forces in Living Cells," *Cell Motility and the Cytoskeleton.,* vol. 52, pp. 97-106, 2002.

19. Parker, K., et. al., "Directional Control of Lamellipodia Extension by Constraining Cell Shape and Orienting Cell Tractional Forces.," *The FASEB Journal.*, vol 16., pp. 1195-1204. 2002.
20. Brock, A., et. al., "Geometric Determinants of Directional Cell Motility Revealed", *Langmuir*, vol 19, pp. 1611-7. 2003.
21. Ingber, D.E., "Tensegrity I. Cell Structure and Hierarchical Systems Biology", *J. Cell Science,* vol 116, pp. 1157-1173, 2003.
22. Satcher, R.L., and Dewey, C.F, "Theoretical Estimates of Mechanical Properties of Endothelial Cell Cytoskeleon.," *Biophys J.* vol 71, pp. 109-118., 1996.
23. Stamenovic D., and Ingber, D.E., "Models of Cytoskeletal Mechanics of Adherent Cells," *Biomech Model Mechanobiol.* vol 1, pp. 95-108, 2002.
24. Vassy, J., et al, "Spatial Distribution of Cytoskeleton Intermediate Filaments During Fetal Rat Hepatocyte Differentiation", *Microscopy Research and Technique,* vol 39. pp. 436-443. 1997.
25. Beil, M., et. al., "A Dual Approach to Structural Texture Analysis in Microscopic Cell Images," *Computer Methods and Programs in Biomedicine,* vol 48, pp. 211-219, 1995.
26. Whitesides, G.M., et al. "Soft Lithography in Biology and Biochemistry," *Annu. Rev. Biomed. Eng.,* Vol 3, pp. 335-373. 2001.
27. Odom, T.W, et. al, "Generation of 30-50nm Structures Using Easily Fabricated, Composite PDMS Masks", *J. Am. Chem Society*, vol 124, pp 12112-12113, 2002.
28. Laibinis, P.E., et. al., "Orthogonal Self-Assembled Monolayers: Alkanethiols on Gold and Alkane Carboxylic Acids on Alumina", *Science,* vol. 245, pp. 845-847. 1989
29. Herrwerth S, et al, "Factors that Determine the Protein Resistance of Oligoether Self-assembled Monolayers -- Internal Hydrophilicity, Terminal Hydrophilicity, and Lateral Packing Density." *J. Am. Chem Soc.* vol 125, pp 9359-9366, 2003.
30. Prime, K., and Whitesides, G.M., "Self-Assembled Organic Monolayers: Model Systems for Studying Adsorption of Proteins at Surfaces." *Science*, vol. 252, pp 1164-167, 1991.
31. So, P.T.C, et. al., "Two-photon Excitation Fluorescence Microscopy," *Annu. Rev. Biomed. Eng.*, Vol 2, pp. 399-429. 2000.
32. Sheetz, M.P. et. al., *Laser Tweezers in Cell Biology*, Academic Press, 1997.
33. Kosta, K.D., "Single-cell Elastography: Probing for Disease with the Atomic Force Microscope.," *Dis Markers*, vol 19, pp. 139-154, 2003.
34. Bausch, A.R., et. al.,"Local Measurements of Viscoelastic Parameters of Adherent Cell Surfaces by Magnetic Bead Microrheometry", *Biophys Journal.,* vol 74. pp. 2038-2049., 1998.
35. Balaban, N.Q., "Force and Focal Adhesion Assembly: A Close Relationship Studied Using Elastic Micropatterned Substrates." *Nature Cell Biology.,* vol 3. pp. 466-472. 2001.
36. Crick, F.H., and Hughes, A.F.W, "The Physical Properties of Cytoplasm: A Study by Means of the Magnetic Particle Method," *Exp. Cell Res.*, vol. 1, pp 37-80, 1949.
37. Wang, N. et. al., "Mechanotransduction Across the Cell Surface and Through the Cytoskeleton", *Science,* vol. 260, pp. 1124-1127, 1993.

38. Bausch, A.R., et. al., "Measurement of Local Viscoelasticity and Forces in Living Cells by Magnetic Tweezers.," *Biophys Journal*, vol 76, pp 573-579. 1999.
39. Huang, H. et. al., "Receptor-based Differences in Human Aortic Smooth Muscle Cell Stiffness, " *Hypertension.,* vol 38, pp. 1158-1161. 2001.
40. Liebovitch, L., *Fractals and Chaos Simplified for the Life Sciences.*, Oxford University Press., 1998.
41. Mandelbrot, B., *Fractal Geometry of Nature.* W.H. Freeman & Co. 1982.
42. Software kindly provided by H. Sasaki, National Institute of Livestock and Grassland Science, Japan.